Dalton Transactions

Knock-on Synthesis of Tritopic Calix[4]pyrrole Host for Enhanced Anion Interactions

Journal:	*Dalton Transactions*
Manuscript ID	DT-ART-06-2019-002365.R1
Article Type:	Paper
Date Submitted by the Author:	11-Jul-2019
Complete List of Authors:	Chahal, Mandeep; National Institute for Materials Science, International Center for Materials Nanoarchitectonics Labuta, Jan; National Institute for Materials Science, International Center for Materials Nanoarchitectonics Březina, Václav; National Institute for Materials Science, International Center for Materials Nanoarchitectonics; Charles University, Faculty of Mathematics and Physics Karr, Paul; Wayne State College, Department of Physical Sciences and Mathematics Matsushita, Yoshitaka; NIMS, Webre, W; University of North Texas, Chemistry Payne, Daniel; University of Birmigham, School of Chemistry Ariga, Katsuhiko; National Institute for Materials Science, World Premier International (WPI) Research Center for Materials Nanoarchitectonics (MANA) D'Souza, Francis; University of North Texas, Chemistry Hill, Jonathan; National Institute for Materials Science, International Center for Materials Nanoarchitectonics

Knock-on Synthesis of Tritopic Calix[4]pyrrole Host for Enhanced Anion Interactions

Mandeep K. Chahal,[1] Jan Labuta,[*1] Václav Březina,[2] Paul A. Karr,[3] Yoshitaka Matsushita,[4] Whitney A. Webre,[5] Daniel T. Payne,[1] Katsuhiko Ariga,[1,6] Francis D'Souza[5] and Jonathan P. Hill[*1]

[1] International Center for Materials Nanoarchitectonics, National Institute for Materials Science, Namiki 1-1, Tsukuba, Ibaraki 305-0044, Japan.

[2] Department of Macromolecular Physics, Faculty of Mathematics and Physics, Charles University, V Holešovičkách 2, 180 00 Prague 8, Czech Republic.

[3] Department of Physical Sciences and Mathematics, Wayne State College, 111 Main Street, Wayne, Nebraska, 68787, USA.

[4] Research Network and Facility Services Division, National Institute for Materials Science (NIMS), 1-2-1 Sengen, Tsukuba, Ibaraki, 305-0047, Japan.

[5] Department of Chemistry, University of North Texas, 1155 Union Circle, 305070 Denton, Texas 76203, USA.

[6] Department of Advanced Materials Science, Graduate School of Frontier Sciences, The University of Tokyo, 5-1-5 Kashiwanoha, Kashiwa, Chiba 277-8561, Japan.

Abstract

Interactions of anionic guests with a tritopic peripherally functionalized conjugated calix[4]pyrrole host (**1**) prepared using a regioselective synthetic method is reported. The regioselectivity of synthesis relies on selective N-alkylation of the calix[4]pyrrole caused by peripheral substitution of one pyrrole group with subsequent N-alkylation at the opposing pyrrole group termed by us 'knock-on' regioselectivity. The resulting host molecule exhibits anion interactions with common chloride and nitrate anions enhanced by an order of magnitude over the parent conjugated calix[4]pyrrole. Combined analysis of ^{1}H-NMR and UV-vis spectroscopic titration data enabled an evaluation of binding strengths of anions with the host K_A in a binding model where the salt dissociation process is also incorporated in the form of its dissociation constant K_d. Anions could be classified as two types based on their interactions with **1**: Type A anions (chloride, nitrate, perchlorate, hydrogensulphate) associate as 1:1 complexes through hydrogen bonding while interactions involving Type B anions (acetate, fluoride, dihydrogenphosphate) are complicated by host deprotonation and/or countercation association. Hosts based on rim-functionalized calix[4]pyrroles such as **1** represent a promising new family of chromophores for estimation of biologically relevant anions or other species.

Introduction

Inorganic anions are an important class of species involved in biological processes[1] or as environmental pollutants.[2] For this reason, they are also important analytes and several methods have been developed for their differentiation, detection and quantification.[3,4] These methods include optical detection using an appropriately functionalized organic chromophore,[5] which can sometimes also be used for differentiation of particular anions,[6-9] where detection and reporting might be based on variation in an inherent physical properties (colour, basicity, etc.).[10] Inorganic oxoanions and polyoxoanions, such as nitrate, hydrogensulphate and perchlorate, have also been studied for their detection using organic molecular reporters[11] and some very elaborate oligomacrocyclic compounds have been designed and synthesized for this purpose.[12,13]

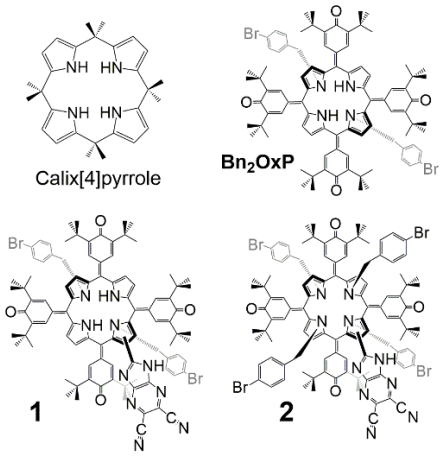

Scheme 1. Chemical structures of calix[4]pyrrole, Bn_2OxP and host molecules **1** and **2** used in this work.

Calix[4]pyrroles[14,15] (Scheme 1) are one of the many types of compound which have been used for the detection of anions and this subject has been studied intensively by Gale,[16] Sessler,[17] Anzenbacher[18] and others.[19] A large family of purpose-built molecules has been synthesized that can bind and report anions including oxoanions[12,13,20] and even anion-cation pairs.[21] The latter

feature has been shown to be important for selective anion extractions[22] and separations.[23] Highly colored calixpyrroles have also been prepared and their use for colorimetric detection of anions reported.[24-29,30-31] In more recent work, we have developed a highly conjugated calix[4]pyrrole whose intense colour in solution and solid states make it suitable for such disclosure-type detection methods. While it has proved of substantial scientific interest for analysis of properties such as solution acidity[28] and solvent hydration[27] in non-polar solvents based purely on its chromogenic properties, its use as an anion sensor has been limited by relatively weak interactions and a resulting lack of specificity.[25] In the present work, we report challenging synthetic adaptations which have been used to overcome this issue. In detail, the introduction of groups in the vicinity of the binding site of a highly conjugated oxoporphyrinogen-type calix[4]pyrrole[32] (this compound is trivially referred to as 'OxP') promotes stronger interactions with oxoanions, which was a particular aim of this work. It has been achieved by using a 'knock-on' regioselective reaction where an initial selective N-alkylation on calix[4]pyrrole is followed by a further regioselective N-alkylation. This has enabled us selectively to prepare rim-functionalized calix[4]pyrroles **1** and **2** capable of interacting tritopically with anionic species. Of course, the resulting complication of the anion binding behaviour has also demanded a consideration of the possible modes of anion binding and we also include a reappraisal of host-guest interactions and salt dissociation based on careful ^{1}H NMR and UV-vis spectroscopic titrations. These matters have revealed the importance of the concentrations of the various interacting species and allowed us to develop a technique for the estimation of anion dissociation constants based on combined analysis of the aforementioned titration data. The new anion host reported here coordinates anions more strongly than the parent macrocycle by an order of magnitude, a factor sufficient for us to consider developing more highly specific anion binding reagents. During the development of our synthesis, we have also discovered a unique spiro-

substituted metalloporphyrin whose crystal structure is included here also to establish the formation of the 1H-imidazo[4,5-b]pyrazine-5,6-dicarbonitrile side-arm in **1** and **2** introduced to improve anion binding properties.

Materials and Methods

General. Reagents and dehydrated solvents (in septum-sealed bottles) used for syntheses were obtained from Tokyo Kasei Chemical Co., Wako Chemical Co. or Aldrich Chemical Co. and were used without further purification. Solvents used for spectroscopic measurements were stored over potassium carbonate to remove traces of acid and filtered just prior to use. Preparative thin layer chromatography (PTLC) was performed using Analtech UNIPLATE™ PTLC silica plates (20 x 20 cm, 1500 microns). Gel permeation chromatography separations were performed with Bio-Beads™ S-X1. Electronic absorption spectra were measured using JASCO V-570 UV/Vis/NIR spectrophotometer, Princeton Applied Research (PAR) diode array rapid scanning spectrometer or a Shimadzu UV/Visible spectrophotometer. FTIR spectra were obtained from solid samples using a Thermo-Nicolet 760X FTIR spectrophotometer. ^{1}H NMR spectra were recorded on a JEOL AL300BX NMR spectrometer at 300 MHz, proton decoupled ^{13}C NMR were recorded at 75 MHz on a JEOL AL300BX NMR spectrometer at the stated temperatures. Data was processed on Delta version 5.0.5.1 and Always JNM-AL version 6.2. ^{1}H NMR chemical shifts (δ) are reported in ppm relative to TMS for $CDCl_3$ (δ = 0.00 ppm) or the residual solvent peak for other solvents. ^{13}C NMR chemical shifts (δ) are reported in ppm relative to the solvent reported. Coupling constants (J) are expressed in Hertz (Hz), shift multiplicities are reported as singlet (s), doublet (d), triplet (t), quartet (q), double doublet (dd), multiplet (m) and broad singlet (bs). Matrix-assisted laser desorption time-of-flight mass spectra (MALDI-TOF-MS) spectra were measured using a Shimadzu-Kratos Axima CR+

spectrometer using dithranol as matrix. Tetrakis(3,5-di-*t*-butyl-4-hydroxyphenyl)porphinatocopper(II) ([T(DtBHP)P]Cu) and tetrakis(3,5-di-*t*-butyl-4-hydroxyphenyl)porphinatonickel(II) were prepared according to a literature method.[33] The synthesis of other intermediates is described in the Supporting Information.

Synthesis

N_{21},N_{23}-Bis(4-bromobenzyl)-2-(5,6-dicyano-1*H*-imidazo[4,5-*b*]pyrazin-2-yl)-5,10,15,20-tetrakis(3,5-di-*tert*-butyl-4-oxo-cyclohexa-2,5-dienylidene)porphyrinogen (1). A mixture of **Bn_2OxP-CHO** (200 mg, 0.13 mmol) and 5,6-diamino-2,3-dicyanopyrazine (86 mg, 0.54 mmol) in dimethylformamide (4 mL) was refluxed for 60 h. After completion of the reaction, the mixture was cooled to room temperature and solvent was removed under reduced pressure. The residue was subjected to column chromatography on SiO_2 eluting with 0.5% acetone in dichloromethane. Product containing fractions were combined and the solvents removed under reduced pressure. The resulting residue was further purified using gel permeation chromatography (BioBeads SX-1) eluting with dichloromethane. Yield: 100 mg (46 %). ^{1}H NMR (300 MHz, $CDCl_3$): δ 9.46 (s, 1H), 9.26 (s, 1H), 7.77 (d, J = 2.2 Hz, 1H), 7.66 (d, J = 2.2 Hz, 1H), 7.60 (d, J = 2.2 Hz, 1H), 7.56 (d, J = 2.2 Hz, 1H), 7.43 (s, 1H), 7.29-7.32 (m, 2H), 7.24 (s, 1H), 6.80-7.11 (m, 10H), 6.48-6.62 (m, 5H), 4.45-4.66 (m, 2H), 4.26-4.38 (m, 2H), 1.21-1.40 (m, 72H) ppm; ^{13}C NMR (76 MHz, $CDCl_3$/acetone-d_6): δ = 186.2, 186.1, 185.2, 159.5, 150.8, 150.8, 149.6, 149.5, 149.3, 149.3, 149.0, 149.0, 148.7, 148.7, 148.0, 142.0, 142.0, 137.5, 136.5, 136.0, 135.8, 134.6, 134.4, 134.1, 133.4, 133.0, 132.9, 132.3, 132.0, 131.6, 131.5, 130.9, 130.5, 130.3, 130.1, 130.0, 129.5, 129.4, 129.3, 128.7, 128.7, 127.0, 125.3, 123.2, 122.4, 120.5, 120.3, 120.0, 119.8, 118.8, 118.8, 113.9, 49.3, 48.6, 36.0, 35.9, 35.8, 35.8, 35.7, 35.5, 35.2, 35.2, 30.6, 30.4, 30.1, 30.1, 29.9, 29.8, 29.6 ppm; FTIR (KBr): ν = 3314.5 (w), 2999.3 (w), 2957.2 (s), 2865.9 (w), 2237.0 (w), 1600.0 (s), 1544.8 (w),

1489.0 (m), 1455.1 (m), 1409.6 (w), 1388.6 (w), 1361.9 (s), 1334.0 (w), 1312.8 (m), 1257.7 (m), 1178.2 (w), 1087.1 (m), 1072.7 (m), 1028.2 (m), 1012.9 (w), 948.2 (m) cm^{-1}; MALDI-TOF-MS (dithranol): calc'd for $[C_{97}H_{102}N_{10}O_4Br_2]^+$ = 1628.64; found: $[C_{97}H_{102}N_{10}O_4Br_2]^+$ = 1628.41 ($[M]^+$).

N_{21},N_{22},N_{23},N_{24}-tetrakis(4-bromobenzyl)-2-(5,6-dicyano-1*H*-imidazo[4,5-*b*]pyrazin-2-yl)-5,10,15,20-tetrakis(3,5-di-*tert*-butyl-4-oxo-cyclohexa-2,5-dienylidene)porphyrinogen (2). Compound **2** was prepared and purified using the same procedure as for **1** with Bn_4OxP-CHO (200 mg, 0.11 mmol) and 5,6-diamino-2,3-dicyanopyrazine (70 mg, 0.44 mmol). Yield: 105 mg (49 %). ^{1}H NMR in $CDCl_3$ (MHz): δ 8.00 (s, 1H), 7.65 (s, 1H), 7.30-7.38 (m, 12H), 7.06-7.20 (m, 4H), 6.85-6.92 (m, 3H), 6.63-6.74 (m, 7H), 6.51-6.56 (m, 3H), 6.15 (d, J = 8.4 Hz, 1H), 4.10-4.86 (m, 8H), 1.24-1.41 (m, 72H) ppm; ^{13}C NMR ($CDCl_3$, 75 MHz): δ 186.1, 185.9, 151.4, 149.3, 149.0, 148.9, 138.7, 137.8, 137.6, 137.6, 136.1, 136.0, 135.3, 132.7, 132.4, 132.3, 132.3, 132.1, 131.9, 130.7, 129.8, 129.7, 129.0, 128.7, 128.4, 128.2, 128.1, 127.7, 126.4, 126.2, 126.1, 123.3, 123.0, 122.9, 122.8, 122.5, 121.2, 120.5, 120.3, 117.0, 116.8, 113.9, 113.8, 48.8, 48.6, 48.1, 48.0, 36.2, 36.1, 35.7, 35.5, 29.9, 29.7, 29.4, 29.1 (ppm); FT-IR(KBr): ν = 2956.9 (s), 2923.9 (m), 2865.5 (w), 2235.6 (w), 1725.1 (m), 1604.7 (s), 1525.4 (w), 1489.0 (m), 1455.0 (m), 1408.5 (w), 1388.4 (w), 1361.3 (M), 1320.5 (m), 1256.4 (w), 1087.7 (m), 1072.6 (m), 1011.9 (m) cm^{-1}; MALDI-TOF-MS (dithranol): calc'd for $[C_{111}H_{114}N_{10}O_4Br_4]^+$ = 1966.57; found: $[C_{111}H_{114}N_{10}O_4Br_4]^+$ = 1966.34 $([M + H])^+$.

X-ray Crystallography. Crystals were grown by slow evaporation of a solution of **3c** in chloroform. Data collection was performed using MoKα radiation (λ = 0.71073 Å) on a RIGAKU VariMax Saturn diffractometer equipped with a charge-coupled device (CCD) detector. Prior to the diffraction experiment the crystal was flash-cooled to 113 K in a stream of cold N_2 gas. Cell refinement and data reduction were carried out using the d*trek program package in the CrystalClear software suite.[34] The

structure was solved using a dual-space algorithm method (SHELXT)[35] and refined by full-matrix least squares on F^2 using SHELXL-2018/1[36] in the WinGX program package.[37] Non-hydrogen atoms were anisotropically refined and hydrogen atoms were placed on calculated positions with temperature factors fixed at 1.2 times Ueq of the parent atoms and at 1.5 times Ueq for methyl groups. Crystallographic data (excluding structure factors) have been deposited with the Cambridge Crystallographic Data Centre with CCDC reference numbers 1920462. Copies of the data can be obtained, free of charge, on application to CCDC, 12 Union Road, Cambridge CB2 1EZ, UK http://www.ccdc.cam.ac.uk/perl/catreq/catreq.cgi, e-mail: data_request@ccdc.cam.ac.uk, or fax: +44 1223 336033. Crystal data for **3c**: Dark green bar, $C_{83.20}H_{90.20}Cl_{10.60}N_{10}NiO_4$, M_r = 1374.23, monoclinic P21/n, a = 18.1354(5) Å, b = 14.6714(4) Å, c = 32.6068(9) Å, β = 97.3260(10)°, V = 8604.9(4) Å^3, *T* = 113 K, Z = 4, R_{int} = 0.0816, GoF = 1.035, R_1 = 0.0658, wR(all data) = 0.1350.

DFT Calculations. DFT calculations at the B3LYP/6-311G(d,p) level were carried out using Gaussian 2016[38] at the Holland Computing Center of the University of Nebraska. Molecular orbital projections were generated using GaussView.[39]

Results and Discussion

Synthesis

The conjugated calix[4]pyrrole Bn_2OxP (Scheme 1) has been studied as a colorimetric probe for anions[25] and enantiomeric excess[40,41] based on its binding site composed of two opposing pyrrolic NH groups at N_{22} and N_{24}. The challenge in this case was to introduce an anion coordinative group at a pyrrole β-position adjacent to the calixpyrrole binding site. This would entail either N-alkylation of an appropriately β-substituted derivative or substitution at the pyrrole β-position of

Bn_2OxP. In order to reach a suitable product either of these reactions would need to proceed with some selectivity in order to facilitate isolation/purification.

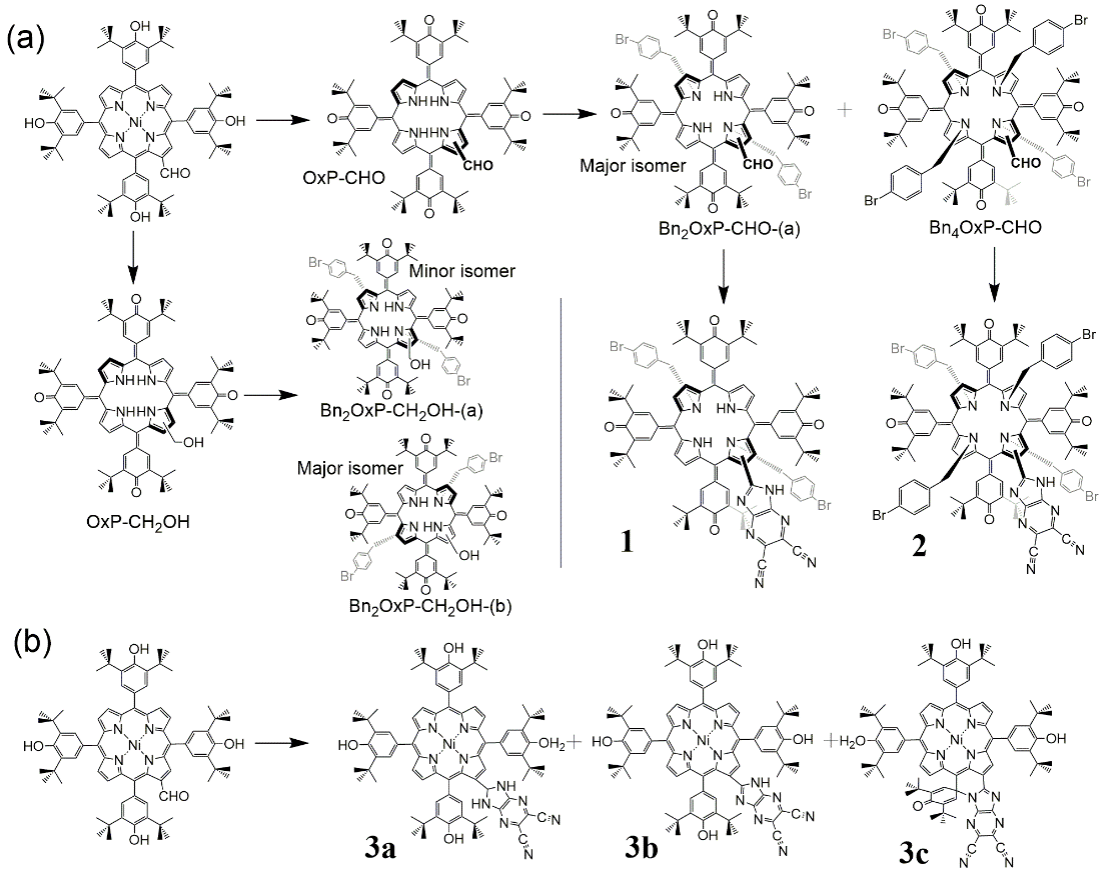

Scheme 2. Development of the 'knock-on' regioselective synthesis of the host molecules. (a) Synthesis of **1** and **2** via Bn_2OxP-CHO-(a) obtained in good yield from the N-benzylation of OxP-CHO. (b) Potential intramolecular reactivity of the 1H-imidazo[4,5-b]pyrazine-5,6-dicarbonitrile substituent illustrated by the formation of compound **3c** (see Scheme 2b, Figure 1).

We selected β-formylation of the macrocycle as being the most useful transformation due to the good yields associated with this reaction on other porphyrin macrocycles and the possibility of its transformation to hydroxymethyl (electron rich) or carboxyl (electron deficient) functionalities. β-Formylation on Bn_2OxP failed. We then considered N-alkylation of the β-substituted macrocycle

where R = hydroxymethyl, formyl or carboxyl (Scheme 2). This reaction builds on our previous observation that di-N-alkylation of OxP occurs leading to N-substitution on one face of the molecule only at N_{21} and N_{23}. Thus, following initial alkylation at N_{21}, the subsequent alkylation occurs regioselectively at N_{23}. This is due either to anion binding at the non-alkylated face of the molecule or tautomerism of the macrocycle which precludes N-alkylation at N_{22} and N_{24}. N-alkylation of OxP-CO_2H gave complex mixtures of products and was not studied further. OxP-CHO and OxP-CH_2OH both gave N-alkylated derivatives that could be isolated. OxP-CH_2OH gave two di-N-substituted compounds while OxP-CHO gave one major di-N-substituted product with another very minor product, which was not isolated. The isomeric identity of these compounds was established by observing the NH resonances in the ^{1}H-NMR spectrum: compounds N-substituted on the β-substituted pyrrole have two NH groups with similar chemical shifts while compounds N-substituted on non-β-substituted pyrrole groups exhibited two widely spaced NH resonances (compare Figures S12 and S14). Connectivity of the N_{21},N_{23}-disubstituted compounds with respect to the β-substituted analogue is also supported by our assignment of NMR spectra of **1** (see Figure S1) using ^{1}H-^{1}H COSY NMR (Figures S2). Thus, the two isomers of Bn_2OxP-CH_2OH could be assigned as Bn_2OxP-CH_2OH-(a) and Bn_2OxP-CH_2OH-(b) with the (a) type isomer having the β-substituent in the required position adjacent to the calix[4]pyrrole binding site but being the product of lower yield. In the case of OxP-CHO, the situation is much simpler with one major product assigned as the (a)-type isomer based on the chemical shifts of NH resonances. The prevalence of the (a)-type isomer is due to the electron withdrawing effect of the formyl group, which increases the reactivity of the NH group of the same pyrrole towards N-alkylation, subsequent N-alkylation then occurs at the opposing pyrrole NH as found previously.[42] These reactions to the (a)-type isomer for OxP-CHO allows almost exclusive synthesis of a precursor containing an appropriately reactive group adjacent to the calixpyrrole

binding site, Bn_2OxP-CHO-(a). We have coined the term 'knock-on regioselectivity' for the synthesis of Bn_2OxP-CHO-(a) since it involves almost selective N-alkylation at N_{21} (due to the presence of β-formyl on that ring) followed by the 'knock-on' regioselective N-alkylation at N_{23} (due to most likely weaker anion binding at that site than occurs at the opposing face of the molecule where anionic guests are doubly H-bonded). For Bn_2OxP-CH_2OH, the type-(b) isomer was preferred and isolation of the type-(a) isomer was not convenient so its synthetic development was ceased. Bn_2OxP-CHO-(a) contains a formyl group that can be subjected to many different transformation procedures. Here we will describe its reaction with a 1,2-phenylenediamines subject to our requirements for the synthetic target. We also note here that non-N-substituted OxP-CHO, which we have also prepared, gave unpredictable and mostly poor results during reactions aimed at its transformation. In this respect, Bn_2OxP-CHO-(a) is a superior intermediate containing a formyl group that reacts predictably according to the reaction conditions applied. In this case, we applied an additional criterion for the β-substituent that it should not contain any aromatic protons since we expected the ^{1}H-NMR spectra of these highly unsymmetrical compounds to be complicated. Therefore, we selected 5,6-diaminopyrazine-2,3-dicarbonitrile as a substrate for condensation with Bn_2OxP-CHO-(a). The structure of the product (**1**) of this reaction is shown in Scheme 2. Note that oxygen was not excluded from the condensation with the result that the product obtained was the corresponding 1H-imidazo[4,5-b]pyrazine-5,6-dicarbonitrile containing an imidazole group in the vicinity of the calixpyrrole binding site. This reaction has been used previously used to prepare β-benzimidazole-substituted metalloporphyrins.[43] The tetra-N-alkylated analogue of **1**, compound **2**, was also prepared in order to assess the anion interaction properties, if any, of the 1H-imidazo[4,5-b]pyrazine-5,6-dicarbonitrile substituent.

Although crystals suitable for X-ray crystallography of **1** and **2** could not be obtained (crystals were not sufficiently stable), a byproduct of the condensation of the metalloporphyin precursor with 5,6-diaminopyrazine-2,3-dicarbonitrile (see Scheme 2b) could be obtained in a suitable form. The compound reveals a 1H-imidazo[4,5-b]pyrazine-5,6-dicarbonitrile moiety joined at the β-pyrrole position as expected but also, interestingly, reveals a further reactivity of the 1H-imidazo[4,5-b]pyrazine-5,6-dicarbonitrile group that is not observed in the oxoporphyrinogen forms. The 1H-imidazo group is fused with the adjacent porphyrin meso-substituent through the carbon atom adjacent to the meso position yielding spiro-type compound **3c** (see Scheme 2b and Figure 1a,b). This is an unusual configuration for the meso substituent, which is present in its hemiquinone state suggesting that its formation is an oxidative process. Molecules of **3c** form π-π dimers (Figure 1c) in the solid state with a short intermolecular closest approach of 3.29 Å (for C42-C44) slightly shorter than the interlayer distance in graphite (3.35 Å) due to the presence of several smaller radii nitrogen atoms. Dimers are arranged in columns running parallel to the *b*-axis (inter-dimer stacking distance: □7.90 Å). This compound is not important for anion binding although its optical properties may be of some interest and will be reported elsewhere. Finally in this section, we note that the final products are racemic mixtures. This aspect will also be addressed in our future reports on the interactions of suitably substituted analogues of these compounds with chiral analytes.

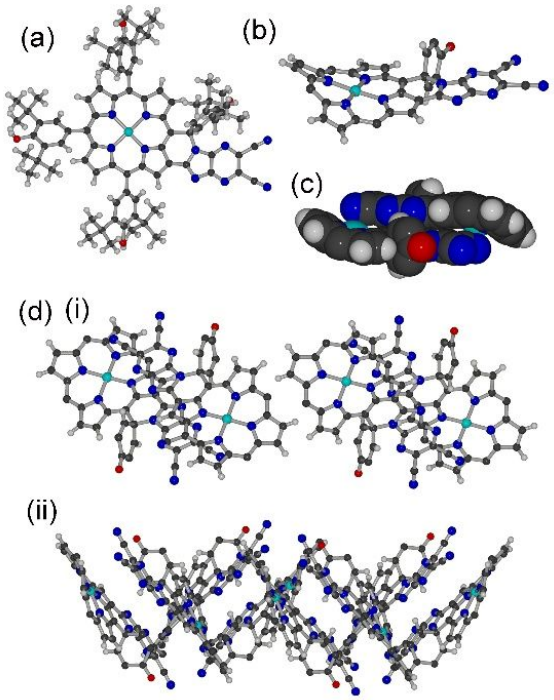

Figure 1. X-ray crystal structure of **3c**. (a) Molecular structure confirming presence of the 1H-imidazo[4,5-b]pyrazine-5,6-dicarbonitrile moiety. (b) Meso-fused structure includes spiro-type linkage of the 4-oxocyclohexa-2,5-dienylidene group. (c) Dimer structure formed by π-π stacking of the fused porphyrin. (d) Columnar structure formed by dimer units, (i) viewed along the *b*-axis, (ii) viewed perpendicular to the *b*-axis. In (b),(c) and (d), meso-substituents and solvent molecules have been removed for clarity.

Computed Structures

In order to assess the different potential interactions of **1** and **2** with anions we first undertook a density functional theory (DFT) study involving the tetraalkylammonium salts of selected anions with the hosts. From these data, assessments can be made of the binding site(s) geometry and various energetic aspects of the interactions that might occur between **1** and **2** and any anionic species in their vicinity.

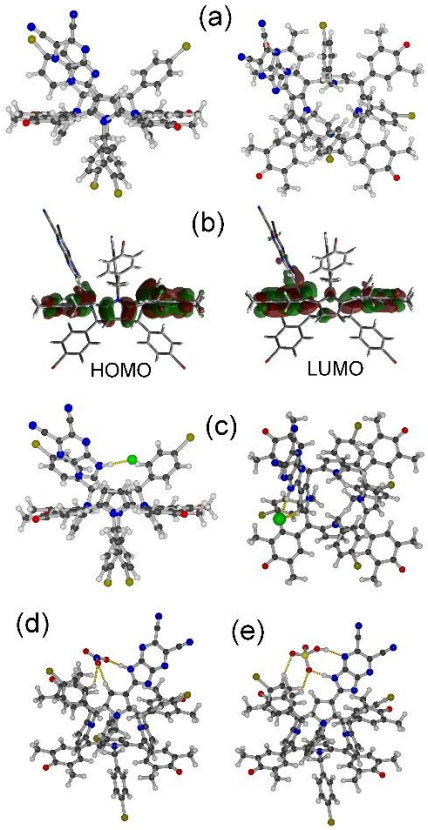

Figure 2. Calculated structure of **2** and several anion complexes. (a) Structure of **2**; note the resemblance with X-ray crystal structures of similar OxP compounds.[25] (b) HOMO and LUMO orbitals for **2**. Notable is only the small contribution from the β-substituent. (c) Structure of the H-bonded complex with chloride anion. (d) Possible H-bonding interactions with nitrate and (e) hydrogensulfate anions.

For **2**, there is apparently a single point for hydrogen-bonding interaction at the benzimidazole NH group. The energy minimized structure of **2** is shown in Figure 2a. The notable structural feature of **2** is coplanarity of the β-substituent with the connected pyrrole group, which is despite there being no contribution to the highest occupied molecular orbital (HOMO; see Figure 2b) from the benzimidazole group. There is, however, a small contribution to the lowest unoccupied molecular orbitals (LUMO) suggesting that the position of the β-substituent affects the molecular orbital structure. Interaction of the imidazo[4,5-b]pyrazine-5,6-dicarbonitrile NH proton leads to a

slight deflection away from coplanarity. Calculations suggest that there is the possibility of deprotonation in the presence of fluoride anions (see also Figure S3, Supporting Information). Also, from our ^{1}H NMR investigations of host-anion responses, basic anions (fluoride, acetate, dihydrogenphosphate) appear to more seriously affect the host compounds **1** and **2** leading to the elimination of resonances due to exchangeable protons. It is unclear whether that observation is due purely to host-guest hydrogen bonding interactions or might be wholly or partly due to deprotonation of the host molecules. For this reason, we have chosen to focus on a selection of anions where ^{1}H NMR peaks due to the host exchangeable protons remain visible in their spectra and can act as probes of host-guest interactions. These anions are chloride, nitrate, perchlorate and hydrogensulphate. Chloride anions are important biochemically while nitrate anions are a widespread environmental contaminant. Perchlorate is an example of a usually weakly interacting anion with hydrogensulphate being capable of donating as well as receiving hydrogen bonds. For **2**, it is also suggested that anions interacting at the benzimidazole group are in a suitable proximity to undergo C-H…A^{-} hydrogen bonding interactions (see Figure 2c-e) with other substituents of the macrocycle (pyrrolic β-H, N-benzylic-H). However, no suitable variation in the ^{1}H NMR spectra could be identified to assess this interaction so that **2** was neglected for further study; anion binding by more sophisticated derivatives of **2** is under investigation.

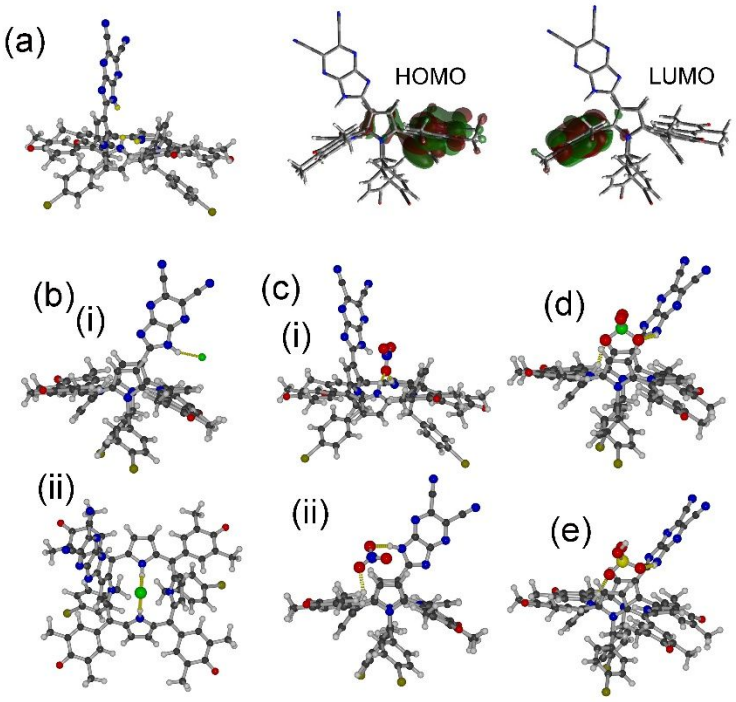

Figure 3. Calculated structures of **1**. (a) Protons depicted in yellow denote the potentially tritopic binding site found in **1**. Distortion of the macrocycle shifts distribution of HOMO and LUMO to opposing sides of the molecule. (b) Chloride anions can bind at (i) benzimidazole NH or (ii) calix[4]pyrrole. (c) Nitrate binds similarly to chloride but can also accommodate bridging modes. Perchlorate (d) and hydrogensulfate (e) also interact at both benzimidazole NH and calix[4]pyrrole binding sites.

For **1**, the complexation scenario is complicated by the presence of two possible binding sites: the same benzimidazole NH group present in **2** and an adjacent calix[4]pyrrole binding site consisting of the two unsubstituted pyrrole NH groups. While for **2**, distortion of the calix[4]pyrrole macrocycle is minimized by the presence of four bulky pyrrole N-substituents, for **1**, the presence of the β-substituent causes deflection of meso-substituents away from coplanarity (see Figure 3a) which affects the molecular orbital structure with HOMO and LUMO found on opposing moieties. Figure 3b-e shows the possible binding modes of **1** with the selected anions chloride (Figure 3b(i,ii)), nitrate (Figire 3c(i,ii)), perchlorate (Figure 3d) and hydrogensulphate (Figure 3e). Importantly,

polyoxoanions appear to undergo multi-topic hydrogen bonding involving bridging between the β-substituent and the calix[4]pyrrole binding site of **1**. This involves twisting of the β-substituent out of coplanarity with the connected pyrrole group. Notably, binding of an anion at the calix[4]pyrrole binding site does not result in changes to the HOMO/LUMO structure of **1** while corresponding interaction at the β-substituent NH leads to donation of electron density into both HOMO and LUMO orbitals. This effect is most pronounced where the benzimidazole group is apparently deprotonated by fluoride anions. For the other anions, hydrogen bonding of the β-substituent NH leads to increasing anionic character of the benzimidazole group indicated by an overall increase in dipole moment (see Figure S4). Binding of anions at the calix[4]pyrrole unit results in slight narrowing of the HOMO-LUMO gap while this parameter is hardly affected by interaction at the β-substituent.

Interactions of Host 1 with Selected Anions

In order to rationalize the binding properties of host **1** with the selected anions (as their tetrabutylammonium (TBA) salts), we have investigated their interactions using ^{1}H NMR and electronic absorption (UV-vis) spectroscopic methods. NMR titration experiments show two different binding behaviors depending on the identity of salt. For TBACl, $TBANO_3$, $TBAClO_4$ and $TBAHSO_4$ salts (Type A; Figures 4a, 5a, S6a and S7a, resp.) the host NH resonances around 9 ppm exhibit downfield shifts while those for TBAOAc, TBAF and $TBAH_2PO_4$ salts (Type B) (Figures S13a, S14a, and S15a) gradually disappear. For the latter Type B salts, this suggests partial or complete deprotonation of the host molecule, which was also partly indicated by several of the DFT calculated structures (see Figures S3, S4 in the ESI). UV-vis titrations of **1** with Type A salts lead to a monotonic

increase of the absorbance maximum centered at 520 nm (Figures 4b, 5b, S6b and S7b, resp.). Type B salts exhibit more complex spectral changes (Figures S13b, S14b, and S15b).

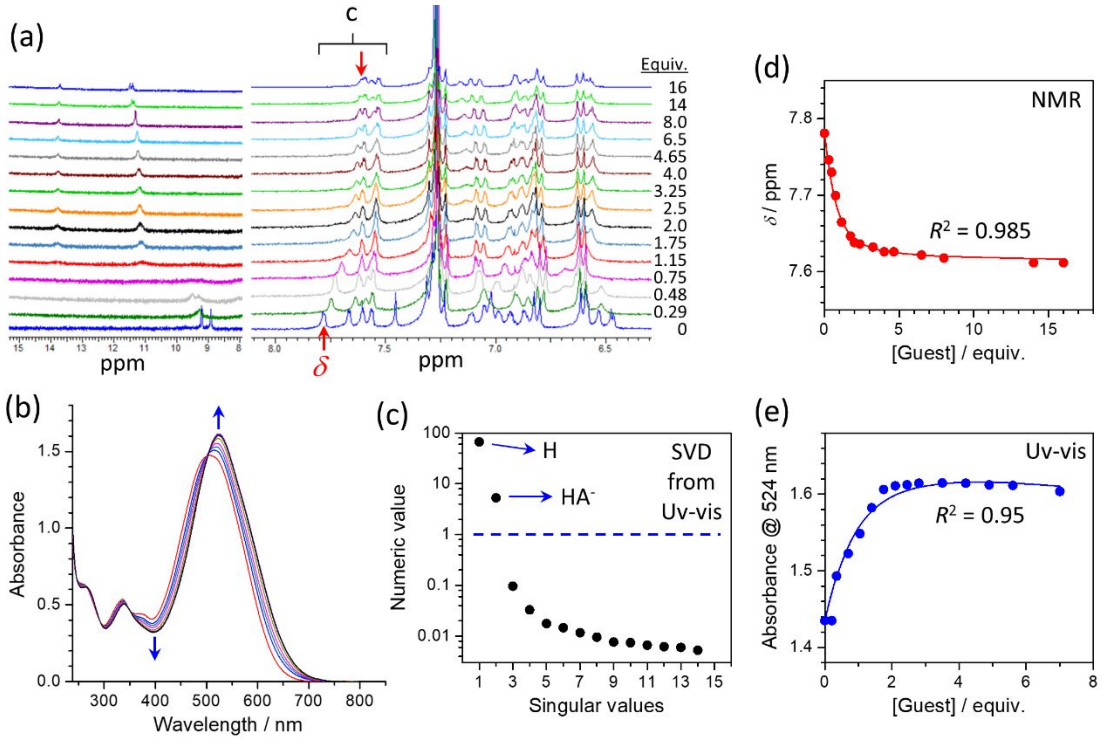

Figure 4. (a) Partial ^{1}H NMR spectra of **1** (2.23×10^{-3} M, $CDCl_3$, 25 °C) during the titration with TBACl (no. of equiv. is denoted at each spectrum). For whole spectra see Figure S5. (b) UV-vis spectra of **1** (1.46×10^{-5} M, CH_2Cl_2, 25 °C) during the titration with 0-7 equiv. TBACl. (c) Singular values as obtained from SVD decomposition of titration in (b) indicate only two significant components (species). (d,e) Experimental binding isotherms (solid circles) as constructed from NMR (resonance at 7.8 ppm) and UV-vis (abs. at 524 nm) titration experiments. Theoretical binding isotherms (solid lines) were constructed from model described in the text and were fitted simultaneously.

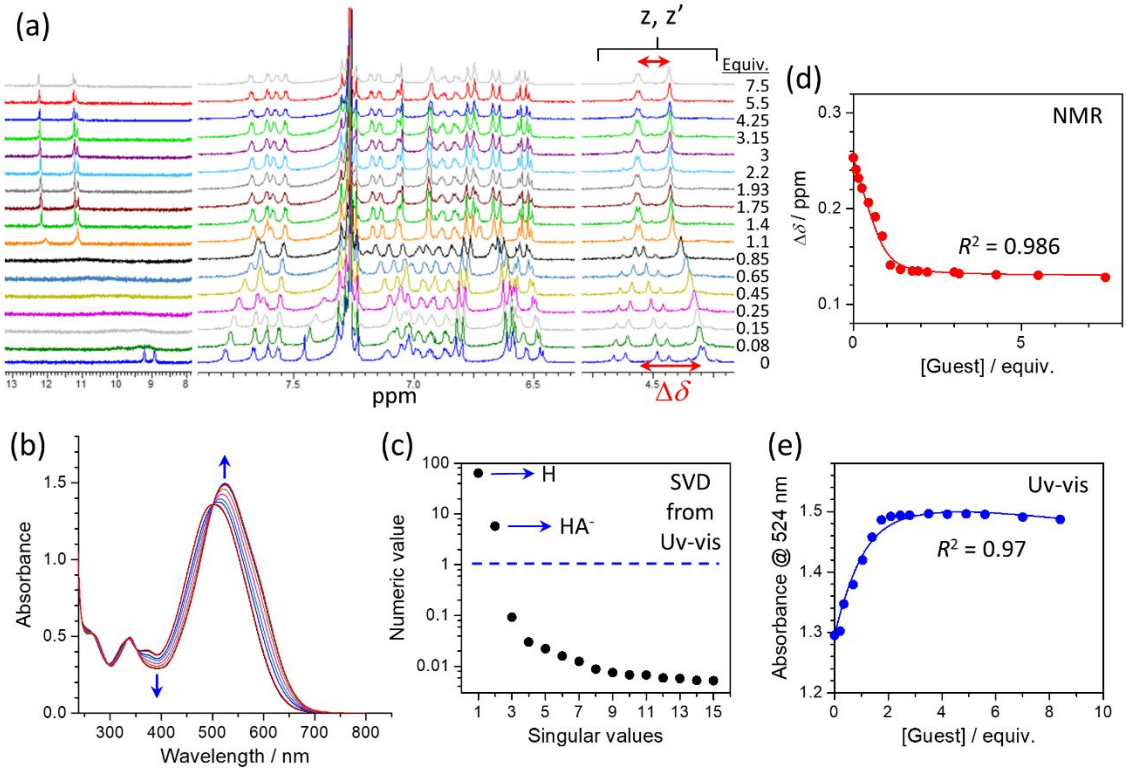

Figure 5. (a) Partial ^{1}H NMR spectra of **1** (2.23×10^{-3} M, $CDCl_3$, 25 °C) during the titration with $TBANO_3$ (no. of equiv. is denoted at each spectrum). (b) UV-vis spectra of **1** (1.46×10^{-5} M, CH_2Cl_2, 25 °C) during the titration with 0-8.4 equiv. $TBANO_3$. (c) Singular values as obtained from SVD decomposition of titration in (b) indicate only two significant components (species). (d, e) Experimental binding isotherms (solid circles) as constructed from NMR (the difference between centers of two resonance at around 4.5 ppm) and UV-vis (abs. at 524 nm) titration experiments. Theoretical binding isotherms (solid lines) were constructed from model described in the text and were fitted simultaneously.

Regarding Type A salts, initially we applied a simple 1:1 host-guest binding model in order to evaluate the binding affinity of **1** (host) to TBA salts (guest). However, the binding constants obtained independently by NMR and UV-vis were not consistent and could not be satisfactorily determined even when both NMR and UV-vis binding isotherms were fitted simultaneously. This indicates that the 1:1 binding model is not capable of an accurate description of complexation processes occurring with these salts. This is due to the assumptions that TBA salts are completely

dissociated when dissolved in non-polar solvents[44] and only free anion (A^-) can interact with host molecule. This apparent discrepancy between NMR (high concentration) and UV-vis (low concentration) titration experiments led us to analyze solely the degree of dissociation (i.e. fraction of free anion) f_A as a function of salt dissociation constant K_d and total salt concentration $[C^+A^-]_t$. Figure 6 shows that for TBACl salt ($K_d = 1.6\times10^{-5}$ M)[45] the fraction of free anion Cl^- varies significantly depending on total concentration. At concentrations used for UV-vis analyses, the salt is relatively well dissociated ($f_A = 0.70$) while, in contrast, at concentrations used for NMR analyses, Cl^- exists largely as an ion-pair ($f_A = 0.12$) with the TBA countercation.

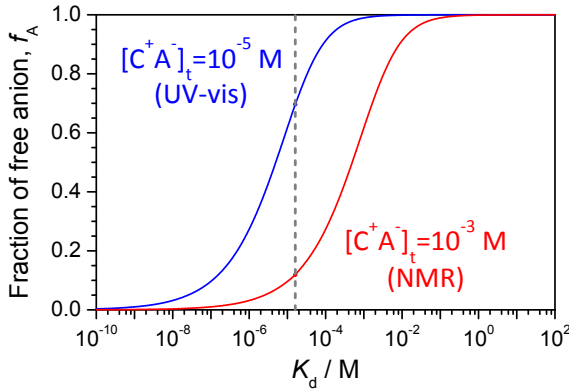

Figure 6. Calculated dependence of fraction of dissociated free anion (f_A) a as function of salt dissociation constant K_d for two total salt concentrations reflecting typical UV-vis (10^{-5} M) and NMR (10^{-3} M) concentrations. The value of $K_d = 1.6 \times 10^{-5}$ M for TBACl in CH_2Cl_2 (at 22 °C)[45] is denoted by gray dashed line.

Therefore, the 1:1 host-anion binding model (Equation 1) was extended to account for the salt dissociation process (Equation 2) in the following manner described by two equilibrium equations:

$$C^+A^- \overset{K_d}{\rightleftharpoons} C^+ + A^- \quad (1)$$

$$H + A^- \overset{K_A}{\rightleftharpoons} HA^- \quad (2)$$

Where H is free host molecule, A^- is free anion, HA^- is host-anion complex and K_A is equilibrium binding constant. C^+A^- is ion-paired (undissociated) salt, C^+ is free cation (i.e. TBA^+) and K_d is salt dissociation constant. The following formulas hold for binding constants and mass and charge balances:

$$K_A = \frac{[HA^-]}{[H][A^-]} \quad (3)$$

$$K_d = \frac{[C^+][A^-]}{[C^+A^-]} \quad (4)$$

$$[H]_t = [H] + [HA^-] \quad (5)$$

$$[C^+A^-]_t = [C^+A^-] + [C^+] \quad (6)$$

$$[C^+A^-]_t = [C^+A^-] + [A^-] + [HA^-] \quad (7)$$

Where square brackets "[ ]"denote the concentration of that species. $[H]_t$ and $[C^+A^-]_t$ denote total analytical concentration of host and salt molecules, respectively. The following formulas can be obtained by algebraic rearrangements of Equations 3-7:

$$[C^+] = [A^-] + K_A[H][A^-] \quad (8)$$

$$[H] = [H]_t/(1 + K_A[A^-]) \quad (9)$$

$$K_{\mathrm{A}}[\mathrm{A}^-]^3 + (1 + K_{\mathrm{A}}[\mathrm{H}]_{\mathrm{t}} + K_{\mathrm{A}}K_{\mathrm{d}})[\mathrm{A}^-]^2 + K_{\mathrm{d}}\left(1 + K_{\mathrm{A}}[\mathrm{H}]_{\mathrm{t}} + K_{\mathrm{A}}[\mathrm{C}^+\mathrm{A}^-]_{\mathrm{t}}\right)[\mathrm{A}^-] - K_{\mathrm{d}}[\mathrm{C}^+\mathrm{A}^-]_{\mathrm{t}} = 0 \quad (10)$$

Solution of Equation 10 using a numerical bisection method yields the concentration of free anion [A^-]. The concentrations of other species, such as [H], [C^+], [C^+A^-] and [HA^-] can be obtained by subsequent evaluation using Equations 9, 8, 4, and 3, respectively. The theoretical NMR and UV-vis binding isotherms have the following forms:

$$\delta = \delta_{\mathrm{H}}[\mathrm{H}]/[\mathrm{H}]_{\mathrm{t}} + \delta_{\mathrm{HA}}[\mathrm{HA}^-]/[\mathrm{H}]_{\mathrm{t}} \quad (11)$$

$$A = \varepsilon_{\mathrm{H}}d[\mathrm{H}] + \varepsilon_{\mathrm{HA}}d[\mathrm{HA}^-] \quad (12)$$

Where δ is the observed NMR chemical shift of a suitable resonance of the host molecule. In some cases, $\Delta\delta$ was used in place of δ, in order to account for the relative shift of two resonances in the spectrum of the host during the titration. δ_{H} and δ_{HA} are the chemical shifts of free host H and host-anion HA^- complex, respectively. *A* is the UV-vis absorbance at a particular wavelength (in figures denoted in subscript), ε_{H} and $\varepsilon_{\mathrm{HA}}$ are the molar extinction coefficients of H and HA^-, respectively. The value of *d* is path length (in cm). Both binding isotherms expressed in Equations 11 and 12 were fitted simultaneously (using a non-linear least squares fitting procedure) in order to account for high (NMR) and low (UV-vis) concentration behaviours.

This model contains only two forms of host molecule, i.e. free H and HA^- complex. In the case of Type A salts, the presence of only two forms of the host **1** is strongly supported by singular value decomposition (SVD) procedure applied to UV-vis titration spectra.[46-49] The SVD procedure can be used to identify the number of components (forms of host molecule) which are present during a titration experiment with a salt (for technical details see ESI). If, for example, only two components are present then the titration data consists only of two different UV-vis spectra, which are present at different proportions (the sum of the proportions is unity). SVD analysis then yields

significant reductions in *numerical values* after the second *singular value*, as can be observed for all Type A salts (Figures 4c, 5c, S6c and S7c, for complete SVD analysis see also Figures S16, S17, S18, and S19). This analysis also supports the use of the above described binding model for Type A salts. In contrast, the SVD analysis of UV-vis titrations of Type B salts indicates the presence of at least three components (i.e. three host forms) (Figures S13b-h, S14b-h, and S15b-h) so that the binding model used for Type A salts cannot be applied. These findings, taken together with NMR titration data for Type B salts (Figures S13a, S14a, and S15a), indicate a rather complicated binding mechanism which probably also involves partial or complete deprotonation of host molecule. While our previous investigations of anion binding with oxoporphyrinogen hosts such as **1** has suggested that deprotonation of the calix[4]pyrrole core only occurs in high polarity solvents such as dimethylsulphoxide, the presence of the 1H-imidazo[4,5-b]pyrazine-5,6-dicarbonitrile group introduces another point for deprotonation especially given the relative electron deficiency of this group and the resulting acidity of its benzimidazole proton. This is supported by the high reactivity of this group when in proximity to meso-substituents leading to the aforementioned oxidative ring fusion activity to the spiro compound **3c**. Increasingly complicated behaviour of host **1** in the presence of Type B salts has prevented us so far from establishing a satisfactory binding model for their interactions.

The analyses of the binding properties of host molecule with different Type A salts were performed by (as mentioned above) simultaneous fitting of NMR and UV-vis binding isotherms. This approach contains high (NMR) and low (UV-vis) concentration behaviours of salts. However, the only literature value of dissociation constant available for TBA salts in CH_2Cl_2 solvent is that for TBACl (K_d = 1.6 $\times$ 10^{-5} M).[45] Therefore, the simultaneous analysis/fitting of the binding isotherms was

performed for various K_d values for each salt. At each value of K_d, the best fit was found and measure of its quality represented as the *total sum of squares* (TSS) was determined (for TBACl see Figure 7a) together with the corresponding binding constant K_A (for TBACl see Figure 7b). The plot of TSS vs. K_d (Figure 7a) exhibits a minimum which is surprisingly close to the literature value for the TBACl dissociation constant. We have estimated an acceptable TSS range for which the quality of fit remains satisfactory (denoted by the gray region in Figure 7a). Correspondingly, the range of acceptable K_A values can also be identified (gray region in Figure 7b). The same analysis was performed for the other Type A salts (Figure 8, S8 and S9) and overall results are represented graphically in Figure 9 with actual values in Table S1.

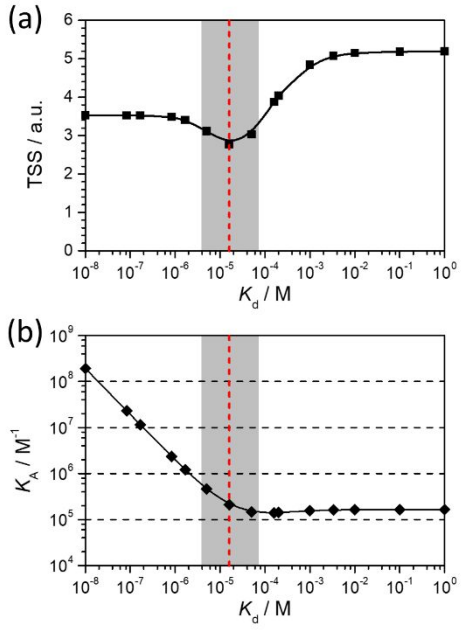

Figure 7. Result of the simultaneous NMR and UV-vis data fitting analysis of **1** with TBACl with variable K_d. (a) Plot of total sum of squares (TSS) dependence on K_d of TBACl. (b) Plot of K_A dependence on K_d. Red dashed lines in (a,b) indicate value of TBACl dissociation constant in CH_2Cl_2 ($K_d = 1.6 \times 10^{-5}$ M).[45] Gray regions denotes acceptable TSS values.

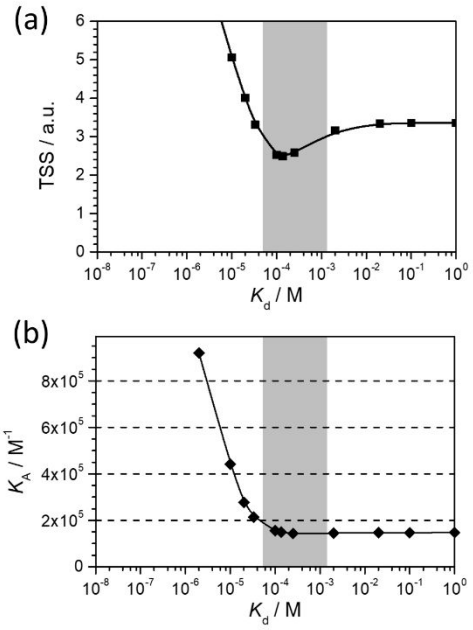

Figure 8. Result of the simultaneous NMR and UV-vis data fitting analysis of **1** with $TBANO_3$ with variable K_d. (a) Plot of total sum of squares (TSS) dependence on K_d of $TBANO_3$. (b) Plot of K_A dependence on K_d. Gray regions denotes acceptable TSS values.

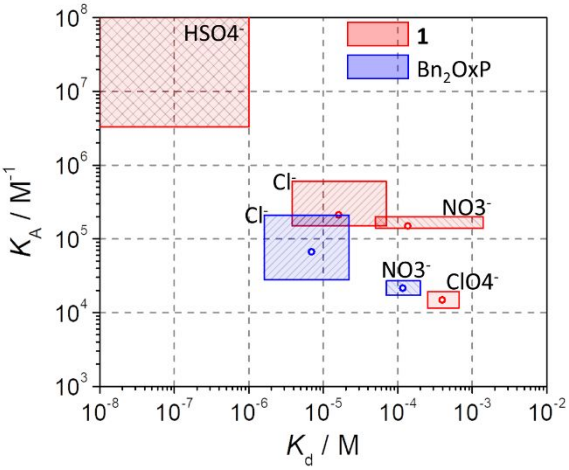

Figure 9. Overall results of binding properties of **1** and Bn_2OxP as obtained from analysis of UV-vis and NMR titration experiments with various anions. Plot of K_A dependence on acceptable values of K_d for all processed combinations of host and anion. Empty circles represent the best fit values.

For comparison, we have also analyzed similarly the binding properties of Bn_2OxP with two of the Type A salts. Data for TBACl salt are shown in Figures 10, S10 and S20 and data for $TBANO_3$ are shown in Supplementary Information Figures S11, S12 and S21. The absence of the 1H-imidazo[4,5-b]pyrazine-5,6-dicarbonitrile group (an anion binding site) from the Bn_2OxP structure reduces the anion binding strength (K_A) by about one order of magnitude (see Figure 9, Table S1).

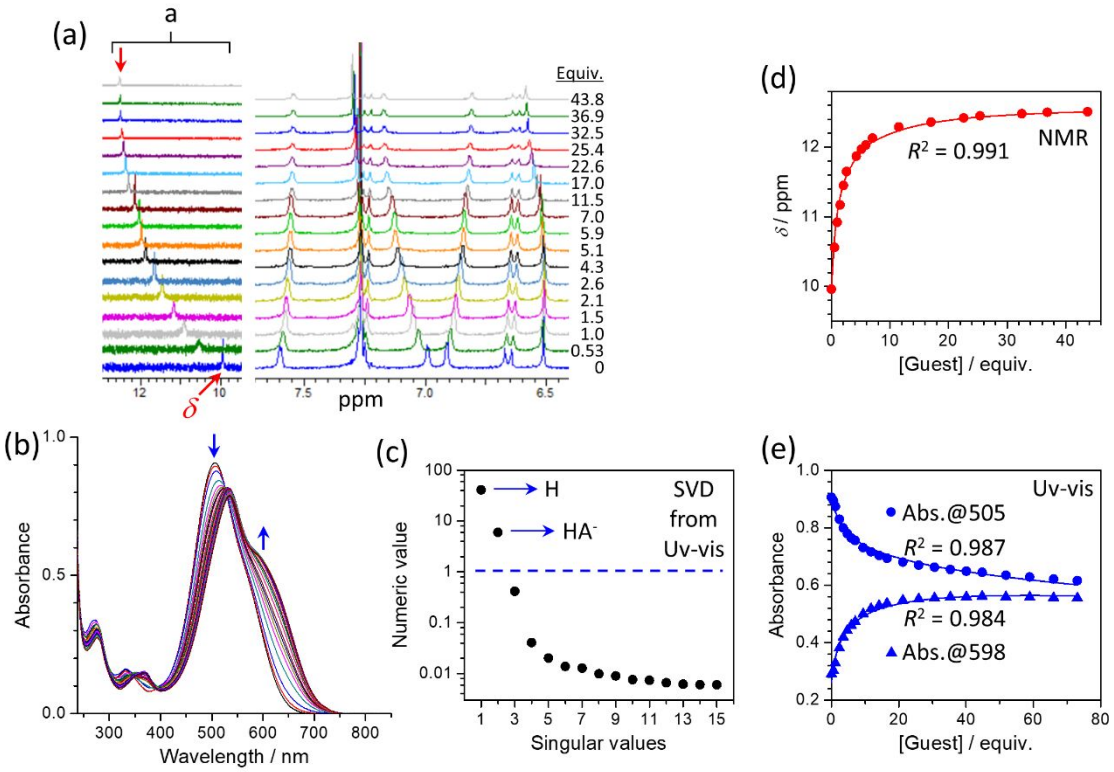

Figure 10. (a) Partial ^1H NMR spectra of Bn_2OxP (2.79×10^{-3} M, $CDCl_3$, 25 °C) during the titration with TBACl (no. of equiv. is denoted at each spectrum). (b) UV-vis spectra of Bn_2OxP (6.15×10^{-6} M, CH_2Cl_2, 25 °C) during the titration with 0-73 equiv. TBACl. (c) Singular values as obtained from SVD decomposition of titration in (b) indicate only two significant components (species). (d,e) Experimental binding isotherms (solid circles) as constructed from NMR (resonance at 10 ppm) and UV-vis (abs. at 505 nm and 598 nm) titration experiments. Theoretical binding isotherms (solid lines) were constructed from model described in the text and were fitted simultaneously.

Discussion

With the recently increasing concern over environmental issues the analysis of various polluting species has become of greater importance. Therefore, methods for improving the potential for detection of analytes by various organic chromophore species has become correspondingly of interest. In this work, we have found that β-functionalization of a highly conjugated calix[4]pyrrole improves the binding qualities of the chromophore for oxoanion species such as nitrate, perchlorate and hydrogensulfate. There is also concomitant improved binding of chloride so that, although differentiation of anions using these molecules is not facilitated, general anion binding properties of the tritopic host **1** have been further optimized over non-substituted Bn_2OxP.

We have also addressed issues of anion binding behaviour in non-polar solvent especially with regard to the mismatch in concentration between two of the commonly used techniques for anion binding studies involving organic species, namely, NMR and UV-vis spectroscopy. Differences in degrees of dissociation of tetra-*n*-butylammonium salts strongly affect the behaviour of the host molecules in solution making a careful consideration of these processes essential in assessing the utility of any potential analytical procedures based on those hosts. Based on data obtained here, we present a means for estimating the dissociation constants of organic salts dissolved in organic solvents using a combination of NMR and UV-vis data (see Figures 7 and 8). This method provides good agreement for the only known value of dissociation constant (for TBACl). The predicted values of dissociation constant for $TBANO_3$ (Figure 8), $TBAClO_4$ (Figure S8) and $TBAHSO_4$ (Figure S9) are given as a range in the simultaneous NMR/UV-vis data fitting analyses. Validation of these data requires further work.

As we have limited our discussion to the Type A salts, the mechanism of anion binding is as expected due largely to hydrogen bonding involving NH groups of the host **1** as indicated by variation in the ^{1}H NMR spectral patterns. Also, all binding models indicate 1:1 host:guest processes for the Type A salts. Resonances due to protons assigned to calix[4]pyrrole NH appear as two reasonably sharp singlets around 9 ppm (see Figure 4 and protons labelled 'a' in Figures S1, S2 with assignment by ^{1}H-^{1}H COSY) while the single proton of the 1H-imidazo[4,5-b]pyrazine-5,6-dicarbonitrile group is not visible in ^{1}H NMR spectra of **1** either because it is obscured by other resonances due to the host or more likely because of exchange processes such as tautomerism, which benzimidazoles are known to undergo[50] and which is probably complicated by the presence of an adjacent fused pyrazine group. A broad resonance appearing subsequent to anion complexation emerging in the region 10 – 14 ppm is assigned to the benzimidazole-type NH proton and has behaviour signifying that it too is involved in anion interactions. That is, data obtained during titration with perchlorate anions, where all three NH peaks (i.e. 2 × calix[4]pyrrole NH and 1 × benzimidazole-type NH) are observable in the spectrum, shift to low field during the titration (see Figure S6). In other cases, this peak appears following saturation of the chemical shift response of the calix[4]pyrrole NH groups. This suggests that initial anion exchange interactions at sub-stoichiometric anion ratios largely involve the calix[4]pyrrole unit while tautomeric processes in the 1H-imidazo[4,5-b]pyrazine-5,6-dicarbonitrile sidearm are only arrested after relatively stable complexation can be attained at stoichiometry above unity (leading to the emergence of its resonance in ^{1}H NMR spectra). An additional feature of NMR spectra is the relative change of chemical shift (while maintaining J-coupling constant; so called 'roof effect') of protons assigned as the N-benzylic methylene groups upon anion binding (see Figure 5a – resonances marked z,z'; Figures S5-S7). These protons appear as geminally coupled second-order doublets of doublets (in the range 4 – 5 ppm) as a result of the

unsymmetrical shielding (by non-equivalent pyrrole groups) and hindered local environment at the calix[4]pyrrole core (see also Figures S1, S2, protons labeled z and z'). Thus, small changes that occur in the calix[4]pyrrole macrocyclic conformation upon anion binding (or solvent binding – see Figure 11 and Figure S1d) cause unsymmetrical variation in the local shielding of the benzylic protons with a resulting variation in the chemical shift of those protons.

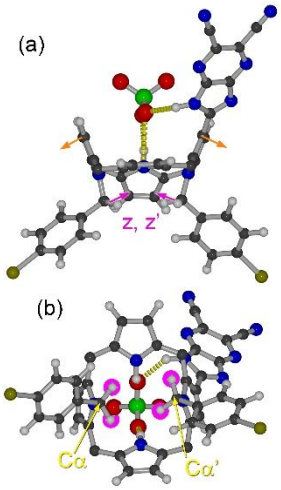

Figure 11. DFT structures indicating sites of variation in conformation of components of host **1**. (a) Perchlorate complex with **1**. Orange arrows indicate the direction of displacement of the pyrrole groups. Pink arrows indicate the resulting displacement of methylene groups with geminally coupled protons z, z' (see Figures S1,S2) leading to variation in their relative chemical shift. (b) Plan view of the N-alkylated face of molecule **1**. Pink circles indicate the positions of z, z' and their non-eqiuvalent environments, which vary on anion binding as benzylic CH_2 groups shift. Inter-CH_2 C_α-$C_{\alpha'}$ distances (DFT): no anion: 4.44 Å; chloride: 3.97 Å; nitrate: 4.33 Å; hydrogensulfate: 4.11 Å; perchlorate: 4.13 Å.

There are two effects to consider: first, changes in dihedral angle between NH-pyrrole groups and macrocycle occurring on guest complexation and, second, variation in the dihedral angle of the N-benzyl pyrrole groups and macrocycle (Figure 11a), which would also cause variation in the local shielding of the benzylic protons (Figure 11b). For the former, NH-pyrrole group dihedral angles

hardly change during anion complexation of Type A anions. However, dihedral angles of N-benzyl pyrrole groups are attenuated by as much as 15° (according to variations in the calculated structures), relocating the corresponding benzyl CH_2 group to a different shielding environment and leading to variation in their relative chemical shift. A measure of this change in structure is given by the distance between benzylic methylene groups on opposing N-atoms, denoted as C_α-$C_{\alpha'}$ (Figure 11b). For non-complexed **1**, C_α-$C_{\alpha'}$ is 4.44 Å and this distance is reduced in anion complexes for chloride (3.97 Å), nitrate (4.33 Å), hydrogensulfate (4.11 Å), and perchlorate (4.13 Å). It is difficult to correlate changes in the geminal protons of benzyl CH_2 group with, for instance, anion identity because structural variations occurring on binding are quite similar from guest to guest. However, it is an interesting effect of the crowded environment in these unsymmetrically substituted calix[4]pyrroles. Finally, it should be noted that, according to DFT calculations, the disposition of one of the pyrrole NH groups is hardly affected by anion interactions although its NH proton appears to remain in close enough proximity to the guest for hydrogen bonding to occur, which is supported by the shifts of both pyrrole NH proton resonances observed in NMR spectra.

Solvent polarity might affect the response of the host molecules. We have confirmed that use of non-polar solvents leads to negligible or less important effects on the absorption spectra of **1** and **2** (Figure S22). In particular, there are only very slight differences between absorption spectra measured in dichloromethane and chloroform (Figure S22b). Polar solvents including DMSO and DMF (Figure S22a) lead to bathochromic shifts and are likely to interfere with anion interactions with the hosts.[25] Molecules similar to **1** have previously also been applied for electrochemical differentiation of anions[51] although this was only effective in the cases of more basic anions such as fluoride. Compounds **1** and **2** behave similarly to those previously reported (Figure S23) so that

electrochemical studies were not carried out here. Finally, we have excluded other halides and pseudohalides such as thiocyanate and azide anions because of their similarities in response with chloride (Figure S24).

Conclusion

In summary, we have prepared new β-functionalized calix[4]pyrrole derivatives based on the Bn_2OxP core chromophore structure. This was made possible by the development of a 'knock-on' regioselective synthesis, which enabled introduction of β-functionality at an appropriate position to improve the anion binding properties of the oxoporphyrinogen 'OxP' chromophore. This synthesis relies on the key intermediate Bn_2OxP-CHO-(a) with a conformation appropriate for the introduction of a wide variety of groups in the vicinity of the versatile calix[4]pyrrole unit. Here, we have exploited this to create a tritopic binding site for anions but Bn_2OxP-CHO-(a) represents an extremely flexible synthon, which we are in the process of developing for different purposes. In this case, anion binding by the resulting host molecule, **1**, is generally an order of magnitude stronger than its parent Bn_2OxP and, in particular, makes these compounds more attractive as hosts for oxoanions. Regarding the anion binding properties of **1**, we have found that it is essential to incorporate the dissociation processes of TBA salts into any complexation models of the salts with OxP-type host molecules such as **1**. The resulting value of equilibrium binding constant K_A of host-anion complexation is largely dependent on the corresponding salt dissociation constant K_d. Therefore, we have also developed a method in which simultaneous fitting of NMR and UV-vis binding isotherms together with analysis of the quality of fit as a function of variable K_d enables a satisfactory determination of both of the important binding parameters, i.e. K_A and K_d. This method

ought also to be of value for application in systems where anions/anion pairs interact with hosts dissolved in organic solvents.

Conflicts of Interest

There are no conflicts of interest to declare.

Acknowledgements

This work was financially supported by the National Science Foundation (Grant No. 1401188 to FD). The study was partially supported by the Grant Agency of Charles University (project GA UK, No. 718214), JSPS KAKENHI Grant No. JP16H06518 (Coordination asymmetry), JSPS KAKENHI Grant No. 19K05229 and CREST JST, Japan (Grant No. JPMJCR1665). D.T.P. is grateful to the Japan Society for the Promotion of Science for a JSPS Fellowship. This work was also partly supported by World Premier International Research Center Initiative (WPI Initiative), MEXT, Japan. The authors are also grateful to the Holland Computing Center of the University of Nebraska, which receives support from the Nebraska Research Initiative, for computation time.

References

1. (a) *Supramolecular Chemistry of Anions*; Bianchi, A.; Bowman-James, K.; Garcia-Espana, E., Eds.; VCH: Weinheim, 1997; (b) R. Martínez-Máñez and F. Sancenón, *Chem. Rev.*, 2003, **103**, 4419.

2. (a) P. Kumar, A. Pournara, K.-H. Kim, V. Bansal, S. Rapti and M. J. Manos, *Prog. Mater. Sci.*, 2017, **86**, 25; (b) B. O. Okesola and D. K. Smith, *Chem. Soc. Rev.*, 2016, **45**, 4226.

3. A. Yamamoto, S. Kodama, A. Matsunaga, Y. Inoue, T. Aoyama and Y. Kumagai, *Chromatography*, 1999, **20**, 116.

4. M. D. Fernándes-Ramos, L. Cuadros-Rodríguez, E. Arroyo-Guerrero and L. F. Capitan-Vallvey, *Anal. Bioanal. Chem.*, 2011, **401**, 2881.

5. (a) P. A. Gale and T. Gunnlaugsson, (Eds) Special themed issue on Supramolecular Chemistry of Anionic Species, *Chem. Soc, Rev.*, 2010, **39**, issue 10; (b) P. A. Gale, *Coord. Chem. Rev.*, 2000, **199**, 181.

6. A. Borissov, I. Marques, J. Y. C. Lim, V. Felix, M. D. Smith and P. D. Beer, *J. Am. Chem. Soc.*, 2019, **141**, 4119.

7. A. Rifai, N. AlHaddad, M. Noun, I. Abbas, M. Tabal, R. Shatila, F. Cazier-Dennin and P. E. Danjou, *Org. Biomol. Chem.*, 2019, **17**, 5818.

8. R. Ali, R. C. Gupta, S. K. Dwivedi and A. Misra, *New. J. Chem.*, 2018, **42**, 11746.

9. G. Men, W. Han., C. Chen., C. Liang and S. Jiang, *Analyst*, 2019, **144**, 2226.

10. (a) B. Gu and Q. Zhang, *Adv. Sci.*, 2018, **5**, 1700609. (b) P.-Y. Gu, Z. Wang and Q. Zhang, *J. Mater. Chem. B*, 2016, **4**, 7060. (c) C. Wang, G. Li and Q. Zhang, *Tetrahedron Lett.*, 2013, **54**, 2633.

11. (a) S. O. Kang, J. M. Llinares, V. W. Day and K. Bowman-James, *Chem. Soc. Rev*., 2010, **39**, 3980; (b) V. Amendola, G. Bergamaschi and A. Miljkovic, *Supramol. Chem.*, 2018, **30**, 236; (c) G. Alibrandi, V. Amendola, G. Bergamaschi, L. Fabbrizzi and M. Licchelli, *Org. Biomol. Chem.*, 2015, **13**, 3510; (d) P. D. Beer and P. A. Gale, *Angew. Chem. Int. Ed.*, 2001, **40**, 486.

12. (a) K. Choi and A. D. Hamilton, *Coord. Chem. Re*v., 2003, **240**, 101; (b) K. Bowman-James, *Acc. Chem. Res*., 2005, **38**, 671.

13. (a) C. R. Rice, C. Slater, R. A. Faulkner and R. L. Allan, *Angew. Chem. Int. Ed.*, 2018, **57**, 13071; (b) J. M. Stauber, G. E. Alliger, D. G. Nocera and C. C. Cummins, *Inorg. Chem.*, 2017, **56**, 7615.

14. (a) D. S. Kim and J. L. Sessler, *Chem. Soc. Rev.*, 2015, **44**, 532; (b) C. H. Lee, *Bull. Kor. Chem. Soc.*, 2011, **32**, 768. (c) P. A. Gale, J. L. Sessler and V. Král, *Chem. Commun*., 1998, **0**, 1. (d) I. Saha, J. T. Lee and C. H. Lee, *Eur. J. Org. Chem.*, 2015, **2015**, 3859.

15. S. Camiolo, P. A. Gale and J. L. Sessler, in *Encyclopedia of Supramolecular Chemistry*, Atwood, J. L.; Steed, J. W., Eds. Marcel Dekker: New York, 2004.

16. (a) P. A. Gale, J. L. Sessler, V. Král and V. Lynch, *J. Am. Chem. Soc.*, 1996, **118**, 5140; (b) P. A. Gale, J. L. Sessler, W. E. Allen, N. A. Tvermoes and V. M. Lynch, *Chem. Commun.*, 1997, **0**, 665.

17. D. S. Kim and J. L. Sessler, *Chem. Soc. Rev.*, 2015, **44**, 532.

18. (a) M. Pushina, P. Koutnik, R. Nishiyabu, T. Minami, P. Savechenkov and P. Anzenbacher, *Chem. Eur. J.*, 2018, **24**, 4879; (b) K.-C. Chang, T. Minami, P. Koutnik, P. Savechenkov, Y. Liu and P. Anzenbacher, *J. Am. Chem. Soc.*, 2014, **136**, 1520.

19. (a) R. Molina-Muriel, G. Aragay, E. C. Escudero-Adan and P. Ballester, *Chem. Commun.*, 2019, **55**, 604; (b) G. Cafeo, G. Carbotti, A. Cuzzola, M. Fabbi, S. Ferrini, F. H. Kohnke, G. Papanikolaou, M. R. Plutino, C. Rosano and A. J. P. White, *J. Am. Chem. Soc.*, 2013, **135**, 2544; (c) R. Dutta, D. Firmansyah, J. Kim, H. Jo, K. M. Ok and C. H. Lee, *Chem. Commun.*, 2018, **54**, 7936.

20. (a) L. Adriaenssens, C. Estarellas, A. Jentzsch Vargas, M. Martinez Belmonte, S. Matile and P. Ballester, *J. Am. Chem. Soc.*, 2013, **135**, 8324; (b) Q. He, M. Kelliher, S. Bahring, V. M. Lynch and J. L. Sessler, *J. Am. Chem. Soc.*, 2017, **139**, 7140.

21. S. K. Kim and J. L. Sessler, *Acc. Chem. Res.*, 2014, **47**, 2525.

22. (a) R. Dutta and P. Ghosh, *Chem. Commun.*, 2014, **50**, 10538; (b) X. Ji, C. Guo, W. Chen, L. Long, G. Zhang, N. M. Khashab and J. L. Sessler, *Chem. Eur. J.*, 2018, **24**, 15791.

23. (a) J. L. Sessler, P. A. Gale and J. W. Genge, *Chem. Eur. J.*, 1998, **4**, 1095; (b) P. A. Gale and C.-H. Lee, *Top. Heterocycl. Chem.*, 2010, **24**, 39; (c) A. Aydogan, D. J. Coady, V. M. Lynch, A. Akar, M. Marquez, C. W. Bielawski and J. L. Sessler, *Chem. Commun.*, 2008, **12**, 1455; (d) R. Custelcean and B. A. Moyer, *Eur. J. Inorg. Chem.*, 2007, 1321; (e) J. Wang, R. G. Harrison and J. D. Lamb, *J. Chromatogr. Sci.*, 2009, **47**, 510; (f) A. El-Hashani, A. Toutianoush and B. Tieke, *J. Phys. Chem. B* 2007, **111**, 8582.

24. R. Nishiyabu, M. A. Palacios, W. Dehaen and P. Anzenbacher, *J. Am. Chem. Soc.*, 2006, **128**, 11496.

25. J. P. Hill, A. L. Schumacher, F. D'Souza, J. Labuta, C. Redshaw, M. R. J. Elsegood, M. Aoyagi, T. Nakanishi and K. Ariga, *Inorg. Chem.*, 2006, **45**, 8288.

26. W. A. Webre, J. P. Hill, Y. Matsushita, P. A. Karr, K. Ariga and F. D'Souza, *Dalton Trans.*, 2016, **45**, 4006.

27. S. Ishihara, J. Labuta, T. Šikorský, J. V. Burda, N. Okamoto, H. Abe, K. Ariga and J. P. Hill, *Chem. Commun.*, 2012, **48**, 3933.

28. A. Shundo, S. Ishihara, J. Labuta, Y. Onuma, H. Sakai, M. Abe, K. Ariga and J. P. Hill, *Chem. Commun*., 2013, **49**, 6870.

29. S. Ishihara, N. Iyi, J. Labuta, K. Deguchi, S. Ohki, M. Tansho, T. Shimizu, Y. Yamauchi, M. Naito, H. Abe, J. P. Hill and K. Ariga, *ACS Appl. Mater. Interfaces.*, 2013, **5**, 5927.

30. M. K. Chahal and M. Sankar, *Dalton Trans.*, 2017, **46**, 11669.

31. M. K. Chahal and M. Sankar, ***Dalton Trans.***, 2016, ***45***, 16404.

32. L. R. Milgrom, *Tetrahedron*, 1983, **39**, 3895.

33. A. J. Golder, L. R. Milgrom, K. B. Nolan and D. C. Povey, *Acta Cryst.*, 1988, **C44**, 1916.

34. *CrystalClear,* Rigaku Corporation, Tokyo, Japan (2005).

35. G. M. Sheldrick, *Acta Cryst.*, 2015, **A71**, 3.

36. G. M. Sheldrick, *Acta Cryst.*, 2008, ***A*64**, 112.

37. L. J. Farrugia, *J. Appl. Cryst.*, 1999, **32**, 837.

38. Gaussian 16, Revision A.03, M. J. Frisch, G. W. Trucks, H. B. Schlegel, G. E. Scuseria, M. A. Robb, J. R. Cheeseman, G. Scalmani, V. Barone, G. A. Petersson, H. Nakatsuji, X. Li, M. Caricato, A. V. Marenich, J. Bloino, B. G. Janesko, R. Gomperts, B. Mennucci, H. P. Hratchian, J. V. Ortiz, A. F. Izmaylov, J. L. Sonnenberg, D. Williams-Young, F. Ding, F. Lipparini, F. Egidi, J. Goings, B. Peng, A. Petrone, T. Henderson, D. Ranasinghe, V. G. Zakrzewski, J. Gao, N. Rega, G. Zheng, W. Liang, M. Hada, M. Ehara, K. Toyota, R. Fukuda, J. Hasegawa, M. Ishida, T. Nakajima, Y. Honda, O. Kitao, H. Nakai, T. Vreven, K. Throssell, J. A. Montgomery, Jr., J. E. Peralta, F. Ogliaro, M. J. Bearpark, J. J. Heyd, E. N. Brothers, K. N. Kudin, V. N. Staroverov, T. A. Keith, R. Kobayashi, J. Normand, K. Raghavachari, A. P. Rendell, J. C. Burant, S. S. Iyengar, J. Tomasi, M. Cossi, J. M. Millam, M. Klene, C. Adamo, R. Cammi,

J. W. Ochterski, R. L. Martin, K. Morokuma, O. Farkas, J. B. Foresman and D. J. Fox, Gaussian, Inc., Wallingford CT, 2016.

39. GaussView, Version 6.0.16, Roy Dennington, T. A. Keith and J. M. Millam, Semichem Inc., Shawnee Mission, KS, 2016.

40. J. Labuta, S. Ishihara, T. Šikorský, Z. Futera, A. Shundo, L. Hanyková, J. V. Burda, K. Ariga and J. P. Hill, *Nat. Commun.*, 2013, **4**, ncomm2188.

41. J. Labuta, J. P. Hill, S. Ishihara, L. Hanykova and K. Ariga, *Acc. Chem. Res.,* 2015, **48**, 521.

42. (a) L. R. Milgrom, J. P. Hill and P. J. F. Dempsey, *Tetrahedron*, 1994, **50**, 13477; (b) J. P. Hill, I. J. Hewitt, C. E. Anson, A. K. Powell, A. L. McCarty, P. A. Karr, M. E. Zandler and F. D'Souza, *J. Org. Chem*., 2004, **69**, 5861; (c) J. P. Hill, W. Schmitt, A. L. McCarty, K. Ariga and F. D'Souza, *Eur. J. Org. Chem*., 2005, 2893.

43. S. Sharma and M. Nath, *J. Hetercycl. Chem.*, 2012, **49**, 88.

44. J. L. Sessler, D. E. Gross, W.-S. Cho, V. M. Lynch, F. P. Schmidtchen, G. W. Bates, M. E. Light and P. A. Gale. *J. Am. Chem. Soc.*, 2006, **128**, 12281.

45. S. Alunni, A. Pero and G. Reichenbach, *J. Chem. Soc., Perkin Trans. 2*, 1998, 1747.

46. E. R. Henry and J. Hofrichter, in *Methods in Enzymology*, Academic Press, 1992, vol. 210, pp. 129–192.

47. E R. Malinowski, Factor Analysis in Chemistry. United States of America, New York: Wiley-Interscience, 2002, pp. 1–432.

48. V. Březina, S. Ishihara, J. Lang, L. Hanyková, K. Ariga, J. P. Hill and J. Labuta, *ChemistryOpen*, 2018, **7**, 323.

49. J. Hanuš, K. Chmelová, J. Štěpánek, P.-Y. Turpin, J. Bok, I. Rosenberg and Z. Točík, *J. Raman Spectrosc.*, 1999, **30**, 667.

50. C. I. Nieto, P. Cabildo, M. Á. Garcia, R. M. Claramunt, I. Alkorta and J. Elguero, *Beilstein J. Org. Chem.*, 2014, **10**, 1620.

51. A. L. Schumacher, J. P. Hill, K. Ariga and F. D'Souza, *Electrochem. Commun.*, 2007, **9**, 2751.